Biomaterials 76 (2016) 408–417

Contents lists available at ScienceDirect

Biomaterials

journal homepage: www.elsevier.com/locate/biomaterials

Method of carrier-free delivery of therapeutic RNA importable into human mitochondria: Lipophilic conjugates with cleavable bonds

Ilya Dovydenko [a, b], Ivan Tarassov [a], Alya Venyaminova [b], Nina Entelis [a, *]

[a] Department of Molecular and Cellular Genetics, UMR Génétique Moléculaire, Génomique, Microbiologie (GMGM), Strasbourg University – CNRS, Strasbourg 67084, France
[b] Laboratory of RNA Chemistry, Institute of Chemical Biology and Fundamental Medicine, Siberian Branch of Russian Academy of Sciences, Novosibirsk, Russia

ARTICLE INFO

Article history:
Received 11 August 2015
Received in revised form
25 October 2015
Accepted 29 October 2015
Available online 31 October 2015

Keywords:
Cell delivery
RNA therapeutics
RNA conjugates
Mitochondrial drug delivery
Mitochondrial diseases
Antireplicative RNA

ABSTRACT

Defects in mitochondrial DNA often cause neuromuscular pathologies, for which no efficient therapy has yet been developed. MtDNA targeting nucleic acids might therefore be promising therapeutic candidates. Nevertheless, mitochondrial gene therapy has never been achieved because DNA molecules can not penetrate inside mitochondria *in vivo*. In contrast, some small non-coding RNAs are imported into mitochondrial matrix, and we recently designed mitochondrial RNA vectors that can be used to address therapeutic oligoribonucleotides into human mitochondria. Here we describe an approach of carrier-free targeting of the mitochondrially importable RNA into living human cells. For this purpose, we developed the protocol of chemical synthesis of oligoribonucleotides conjugated with cholesterol residue through cleavable covalent bonds. Conjugates containing pH-triggered hydrazone bond were stable during the cell transfection procedure and rapidly cleaved in acidic endosomal cellular compartments. RNAs conjugated to cholesterol through a hydrazone bond were characterized by efficient carrier-free cellular uptake and partial co-localization with mitochondrial network. Moreover, the imported oligoribonucleotide designed to target a pathogenic point mutation in mitochondrial DNA was able to induce a decrease in the proportion of mutant mitochondrial genomes. This newly developed approach can be useful for a carrier-free delivery of therapeutic RNA into mitochondria of living human cells.

1. Introduction

Small RNA molecules are increasingly used in clinical applications. RNA-based therapeutics include inhibitors of mRNA translation, agents of RNA interference, ribozymes and aptamers binding various molecular targets [1,2]. Recently, we developed mitochondrial RNA vectors that can be used to address therapeutic oligoribonucleotides into human mitochondria [3,4]. To date, >250 human diseases, mostly neuromuscular and neurodegenerative, were shown to be caused by defects in mitochondrial DNA (mtDNA) [5]. The majority of these mutations are heteroplasmic, meaning that mtDNA coexists in two forms, wild type and mutated, in the same cell. The occurrence and severity of pathologic effects depend on the heteroplasmy level, therefore, the shift in proportion between two types of mitochondrial genome could restore mitochondrial functions [6,7]. Anti-replicative strategy aims to decrease the heteroplasmy level by targeting into mitochondria the RNA molecules able to affect the replication of mutant mtDNA. Recently, we demonstrated that small RNAs containing structural determinants for mitochondrial import (hairpin domains responsible for RNA mitochondrial targeting) and 20-nucleotide sequence corresponding to the mutated region of mtDNA, are able to anneal selectively to the mutated mitochondrial genomes. Capable to penetrate into mitochondria of cultured human cells, these RNAs induced a decrease of the proportion of mtDNA bearing pathogenic mutations [4,8].

A factor that significantly limits biomedical application of RNAs is their inefficient delivery to target cells and tissues due to large size, negative charge and low stability of the molecules [9]. A frequently used approach of therapeutic RNA delivery in the complexes with commercial cationic lipids (as, for instance, Lipofectamine) had been characterized by high toxicity and inefficiency *in vivo* and, therefore, is not suitable for therapeutic applications

* Corresponding author. UMR 7156, 4, Allée Konrad Roentgen, 67084 Strasbourg Cedex, France.
E-mail address: n.entelis@unistra.fr (N. Entelis).

http://dx.doi.org/10.1016/j.biomaterials.2015.10.075

[10]. The conjugation of RNA with the ligands which can be internalized by natural transport mechanisms is a promising approach to overcome this problem [11].

To decrease the toxicity of cell transfection procedure and create an approach of targeting various anti-replicative RNAs into living human cells, we designed conjugates containing a cholesterol residue. Cholesterol is a natural lipid and an essential structural component of animal cell membranes, its efficiency as a transporter molecule and low toxicity were demonstrated by several research groups [12–14]. Nevertheless, cholesterol could stall the mitochondrial import of therapeutic anti-replicative RNA due to attachment to the mitochondrial membranes. To address this problem, we synthesized RNA molecules conjugated with cholesterol through biocleavable covalent bonds. These linkages have been previously used to release drugs under specific conditions: cleavage of disulfide bonds is triggered by a mildly reducing intracellular environment; hydrazone bonds are pH-triggered linkers releasing the drug in acidic conditions of endosomes [15]. Here we describe the synthesis of oligoribonucleotides conjugated with cholesterol through cleavable covalent bonds and show that this approach can be used for a carrier-free transfection of human cells with anti-replicative RNA molecules addressing mtDNA mutations.

2. Materials and methods

2.1. Chemical compounds

Thiol-Modifier C6 S-S, 5′-Aldehyde-Modifier C2, RNA phosphoramidites and solid supports for oligoribonucleotide synthesis were obtained from Glen Research; cholesteryl chloroformate, 6-aminohexanoic acid, cysteamine, chloroquine diphosphate salt and FITC isomer I were purchased from Sigma–Aldrich; hydrazine hydrate from Fluka; ATTO 565 N-succinimidyl ester from ATTO-TEC. Other chemicals were supplied by Merck, Acros and TCI. Solvents were supplied by Panreac.

2.2. Synthesis of chemical compounds

2.2.1. 6-(Cholesteryloxycarbonylamino)-hexanoic acid (**1**)

Compound (**1**) (Fig. 1A, step i) was synthesized as described in Ref. [16] with modifications. 6-Aminohexanoic acid (0.9 g, 6.6 mmol) was suspended in dry pyridine (15 ml), then chlorotrimethylsilane (3.3 ml, 26.4 mmol) was added dropwise at 0 °C. The mixture was stirred until the solution became clear, then cholesteryl chloroformate (1 g, 2.2 mmol) was added and the reaction mixture was stirred for 3 h at room temperature. Pyridine was evaporated under reduced pressure, the residue was dissolved in dichloromethane (100 ml), washed with 0.7 M hydrochloric acid (50 ml) and saturated aqueous NaCl (50 ml). The organic phase was dried under anhydrous Na_2SO_4 and evaporated under reduced pressure. The residue was purified by Silica gel, pore size 60 Å, 230–400 mesh (Sigma) column chromatography (CH_2Cl_2/EtOH, 0–30%) to obtain (**1**) with a yield 0.95 g (80%). ^{1}H NMR spectra were recorded on a Bruker AV-400 spectrometer with tetramethylsilane as an internal standard. H^1-NMR (400 MHz, $CDCl_3$, δ, ppm): 0.69 (s, 3H, H-18/19 cholesterol); 0.87 (d, 3H, H-26/27 cholesterol); 0.89 (d, 3H, H-26/27 cholesterol); 0.93 (d, 3H, H-21 cholesterol); 1.025 (s, 3H, H-18/19 cholesterol); 2.33 (t, 2H, $-C\underline{H}_2-COOH$); 3.35 (dd, 2H, $-C\underline{H}_2-NH-$); 4.51 (m, 1H, H-3 cholesterol); 4.88 (t, 1H, –NH–); 5.4 (d, 1H, H-6 cholesterol).

2.2.2. Methyl 6-(cholesteryloxycarbonylamino)hexanoate (**2**)

Compound (**1**) (0.2 g, 0.37 mmol) was dissolved in dry dichloromethane (5 ml), phosphorus trichloride (13 μl, 0.149 mmol) was added (Fig. 1A step ii), the reaction mixture was stirred for 3 h under argon at 50 °C, then absolute methanol (1 ml) was added. The mixture was diluted by dichloromethane (45 ml) and washed with saturated aqueous $NaHCO_3$ (50 ml) and twice by water (50 ml). The organic phase was dried under anhydrous Na_2SO_4 and evaporated to oily residue. The product (**2**) was purified by Silica gel column chromatography (CH_2Cl_2/EtOH, 0–2.5%) (yield 0.165 g, 80%).

H^1-NMR (400 MHz, $CDCl_3$, δ, ppm): 0.69 (s, 3H, H-18/19 cholesterol); 0.87 (d, 3H, H-26/27 cholesterol); 0.89 (d, 3H, H-26/27 cholesterol); 0.93 (d, 3H, H-21 cholesterol); 1.025 (s, 3H, H-18/19 cholesterol); 2.29 (t, 2H, $-C\underline{H}_2-C(O)OCH_3$); 3.35 (dd, 2H, $-C\underline{H}_2-NH-$); 3.65 (s, 3H, $-CH_2-C(O)OC\underline{H}_3$); 4.51 (m, 1H, H-3 cholesterol); 4.88 (t, 1H, –NH–); 5.4 (d, 1H, H-6 cholesterol).

2.2.3. Hydrazine 6-(cholesteryloxycarbonylamino)hexanoate (**3**)

Hydrazine derivative (**3**) was synthesized by analogy with [17]. Compound (**2**) (0.1 g, 0.18 mmol) was dissolved in methanol (5 ml). Hydrazine monohydrate (1.25 ml, 49 mmol) was added dropwise (Fig. 1A step iii), and the reaction mixture was left for 8 h at room temperature. Compound (**3**) was precipitated in cold water (100 ml), the precipitate was filtered off, washed with water and dried (yield, 0.089 g, 89%). H^1-NMR (400 MHz, $CDCl_3$, δ, ppm): 0.69 (s, 3H, H-18/19 cholesterol); 0.87 (d, 3H, H-26/27 cholesterol); 0.89 (d, 3H, H-26/27 cholesterol); 0.93 (d, 3H, H-21 cholesterol); 1.025 (s, 3H, H-18/19 cholesterol); 2.13 (t, 2H, $-C\underline{H}_2-C(O)NH-NH_2$); 3.35 (dd, 2H, $-C\underline{H}_2-NH-$); 3.85 (s, 2H, $-CH_2-C(O)NH-N\underline{H}_2$); 4.51 (m, 1H, H-3 cholesterol); 4.88 (t, 1H, –NH–); 5.4 (d, 1H, H-6 cholesterol); 6.75 (s, H, $-CH_2-C(O)N\underline{H}-NH_2$).

2.2.4. 2-(Pyridyldithio)-ethylamine (**4**)

Compound (**4**) (Fig. 1B step i) was synthesized as described in Ref. [18] with some modifications. The reaction was kept under argon atmosphere. Cysteamine (0.23 g, 2 mmol) was dissolved in methanol (5 ml) and added dropwise to a stirred solution of 2,2′-dipyridyl disulfide (0.88 g, 4 mmol) in methanol/acetic acid (1:25; 4 ml). The mixture was stirred at room temperature for 48 h and then evaporated to oily residue. The product (**4**) was precipitated by cold diethyl ether (20 ml), suspension was filtered and the precipitation step was repeated three times. H^1-NMR (400 MHz, D_2O, δ, ppm): 3.1 (m, 2H, $NH_2-C\underline{H}_2-CH_2-S-$); 3.29 (t, 2H, $NH_2-CH_2-C\underline{H}_2-S-$); 7.3 (m, 1H, 3′-H, pyridyl); 7.74 (m, 1H, 4′/5′-H, pyridyl); 7.81 (m, 1H, 4′/5′-H, pyridyl); 8.4 (m, 1H, 6′-H, pyridyl).

2.2.5. Cholesteryl N-[2-(2-pyridyldisulfonyl)ethyl]carbamate (**5**)

Synthesis of (**5**) was carried out as described in Ref. [19] with some modifications (Fig. 1B step ii). To the cholesteryl chloroformate solution (0.4 g, 0.9 mmol) in dry dichloromethane (4 ml), were added the suspension of (**4**) (0.1 g, 0.45 mmol) in dioxane (2 ml) and triethylamine (0.15 ml, 1.1 mmol). The reaction mixture was stirred for 48 h under argon at room temperature. After addition of dichloromethane (20 ml), reaction mixture was washed twice with saturated aqueous $NaHCO_3$ (20 ml) and water (20 ml). The organic phase was dried under anhydrous Na_2SO_4 and evaporated to oily residue. The product (**5**) was purified by Silica gel column chromatography (hexane/ethyl acetate, 0–30%) (yield 0.19 g, 71%). H^1-NMR (400 MHz, $CDCl_3$, δ, ppm): 0.69 (s, 3H, H-18/19 cholesterol); 0.87 (d, 3H, H-26/27 cholesterol); 0.89 (d, 3H, H-26/27 cholesterol); 0.93 (d, 3H, H-21 cholesterol); 1.025 (s, 3H, H-18/19 cholesterol); 2.92 (dd, 2H, $-NH-C\underline{H}_2-CH_2-S-$); 3.44 (m, 2H, $-NH-CH_2-C\underline{H}_2-S-$): 4.47 (m, 1H, H-3 cholesterol); 4.88 (t, 1H, –NH–); 5.35 (d, 1H, H-6 cholesterol); 7.1 (m, 1H, 3′-H, pyridyl); 7.51 (m, 1H, 4′/5′-H, pyridyl), 7.59 (m, 1H, 4′/5′-H, pyridyl); 8.51 (m, 1H, 6′-H, pyridyl).

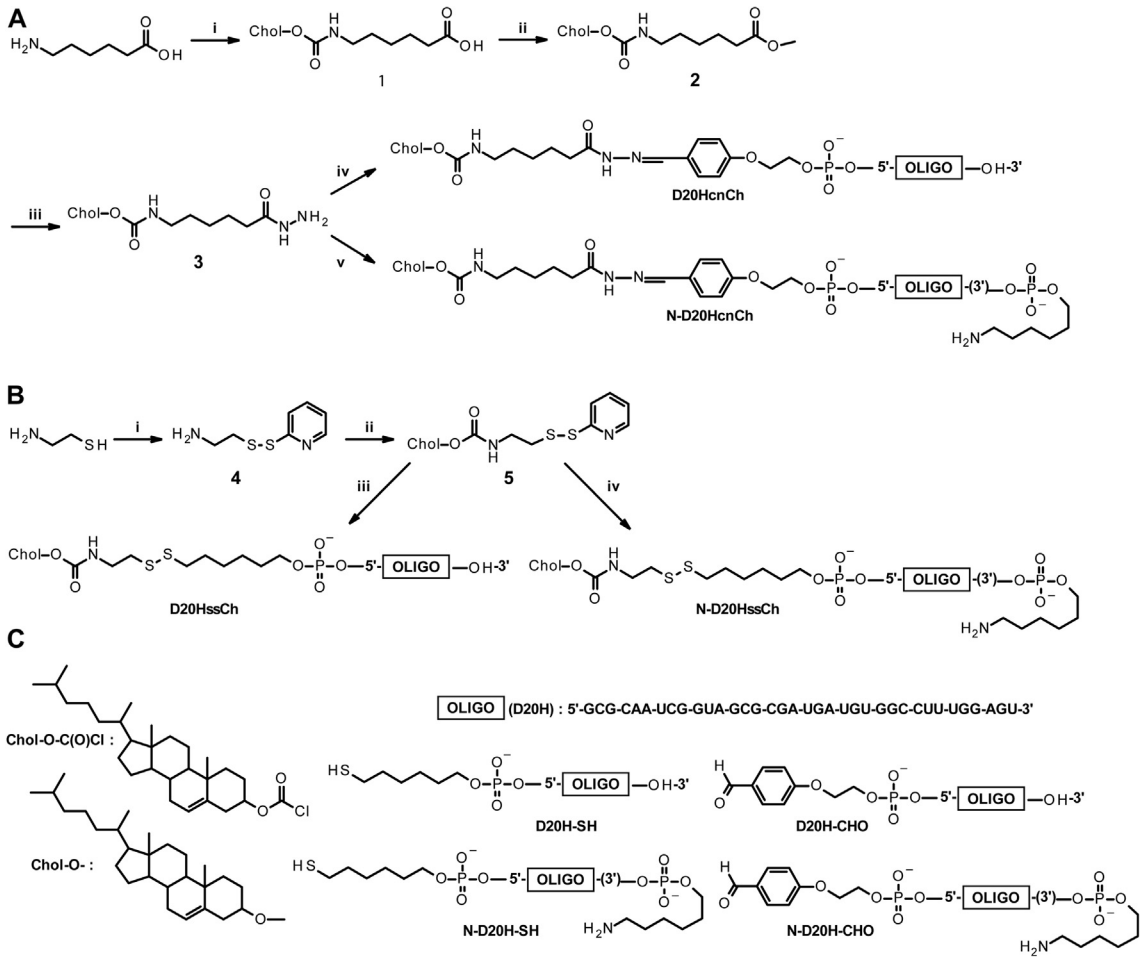

Fig. 1. Synthesis of oligoribonucleotides conjugated with cholesterol through cleavable covalent hydrazone (A) and disulfide (B) bonds. Reagents: A, i) $(CH_3)_3SiCl$, Py, 4°C; CholOC(O)Cl, Py, r.t.; H_3O^+; ii) PCl_3, CH_2Cl_2, argon, 50°C; $MeOH_{abs}$, r.t.; iii) $NH_2NH_2 \cdot H_2O$, MeOH, r.t.; iv) D20H-CHO, 0.1 M NaOAc, pH 5.0/dioxane, r.t.; v) N-D20H-CHO, 0.1 M NaOAc, pH 5.0/dioxane, r.t.; B. i) $(PyS)_2$, MeOH/AcOH, r.t.; ii) CholOC(O)Cl, CH_2Cl_2/dioxane/Et_3N, argon, r.t.; iii) D20H-SH, dioxane, r.t.; iv) N-D20H-SH, dioxane, r.t. C. Structure of compounds used for the synthesis.

2.3. Oligonucleotide synthesis

Oligoribonucleotide D20H (Fig. 1C) was synthesized on an automatic DNA/RNA ASM-800 synthesizer (Biosset) at 0.4 μmol scale using 2′-O-TBDMS-protected phosphoramidites and solid phase phosphoramidite synthesis protocols [20] optimized for the instrument. Synthesis of 3′-amino modified oligoribonucleotide (N-D20H) was carried out using 3′-PT-Amino-Modifier C6 CPG (Glen Research). At the final step of the synthesis, Thiol-Modifier C6 S-S or 5′-Aldehyde-Modifier C2 phosphoramidites were used. Cleavage of oligoribonucleotides from the support and removal of 2′-O-silyl and nucleobase exocyclic amine protecting groups were carried out as described previously [13].

2.4. Synthesis of lipophilic conjugates with hydrazone bond (D20HcnCh and N-D20HcnCh)

Modified with 5′-Aldehyde-Modifier C2 phosphoramidite oligoribonucleotides D20H and N-D20H were incubated in 80% acetic acid 1 h at room temperature to remove the acetal protecting group, then oligoribonucleotides were precipitated by addition of 2% $NaClO_4$ in acetone and isolated via preparative electrophoresis in 12% polyacrylamide/8 M urea gel (acrylamide:N,N′-methylenebisacrylamide 30:0.5, TBE buffer, 10 V/cm) followed by elution with 0.3 M NaOAc (pH 5.2)/0.1% SDS solution and precipitation with ethanol. Purified oligoribonucleotides D20H–CHO and N-D20H–CHO were conjugated with compound (**3**) (Fig. 1A steps iv, v). For this, the oligoribonucleotides (5 units A_{260}) dissolved in 50 μl of 0.1 M NaOAc pH 5.0 were mixed with the same volume of (**3**) (3 mg, 5.2 μmol) in dioxane and incubated 12 h at room temperature with permanent stirring. Yield of the products D20HcnCh and N-D20HcnCh was estimated by gel electrophoresis and ethidium bromide staining as a ratio between signals corresponding to product (D20HcnCh or N-D20HcnCh) and initial compound (D20H–CHO or N-D20H–CHO). Cholesterol-conjugated oligoribonucleotides D20HcnCh and N-D20HcnCh were characterized by ESI-TOF-MS analysis (theoretical mass 12405.8 Da, measured mass 12405.2 Da) performed by the Proteomics Platform of Esplanade, Strasbourg, France.

2.5. Synthesis of lipophilic conjugates with disulfide bond (D20HssCh and N-D20HssCh)

Modified with Thiol-Modifier C6 S–S phosphoramidite (Glen Research) oligonucleotides D20H and N-D20H (5 units A_{260}) were treated with 50 mM DTT, 25 mM HEPES–NaOH, pH 8.5 at room temperature for 30 min with permanent stirring, precipitated with 2% $NaClO_4$ in acetone, the pellet was washed with acetone and

dried. The reduced 5′-thiol containing oligonucleotide derivatives D20H-SH and N-D20H-SH (Fig. 1C) were purified using Bio-Rad P6 column in 100 mM HEPES–NaOH, pH 8.5, for complete elimination of DTT.

Compound (**5**) (2 mg, 3.3 μmol) in dioxane (0.2 ml) was added to 5′-thiol oligonucleotide and incubated overnight at room temperature with permanent stirring (Fig. 1B steps iii, iv), followed by precipitation with 2% $NaClO_4$ in acetone. Cholesterol-conjugated oligoribonucleotides D20HssCh (yield 30%) and N-D20HssCh (yield 45%) (yields were estimated as described above) were isolated via preparative electrophoresis in 12% polyacrylamide/8 M urea gel, followed by elution with 0.3 M NaOAc (pH 5.2)/0.1% SDS solution and precipitation with ethanol. The purified D20HssCh and N-D20HssCh were characterized by ESI-TOF-MS analysis (theoretical mass 12320.4 Da, measured mass 12321.0 Da).

2.6. Synthesis of fluorescently labelled conjugates

Labelling of lipophilic conjugates with ATTO-565 or FITC was carried out as described previously [21]. Briefly, the conjugate containing 3′-terminal aminolinker (N-D20HssCh or N-D20HcnCh) (5 units A_{260}) dissolved in 85 μl of 0.1 M HEPES–NaOH, pH 8.5 was mixed with 15 μl of *N*-succinimidyl ester of ATTO-565 in dry DMSO (5 mg/ml); or (N-D20HcnCh) (1 unit A_{260}) in 30 μl of 0.1 M HEPES–NaOH, pH 8.5 was mixed with 30 μl of FITC dissolved in dry DMSO (10 mg/ml). Reaction mixture was incubated overnight at room temperature with permanent stirring. The conjugates were precipitated with ethanol as Na^+ salts.

2.7. Test of the lipophilic conjugates stability

To test the hydrazone bond stability, 100 ng of D20HcnCh conjugate was incubated for 2.5, 4, 6, 8 and 24 h at 37 °C in 20 mM Na-acetate buffer pH 4.6; 5.2 or 5.6 or Na-phosphate buffer pH 6.0; 6.6 or 7.4. Stability of D20HssCh was tested in 20 mM Hepes–NaOH, pH 7.4 containing 5 mM glutathione (GSH) 3 h at 37 °C. For complete reduction of the disulfide bond, the conjugate was incubated with 20 mM β–mercaptoethanol 15 min at room temperature.

Reaction products were separated on 8 M urea – 12% PAGE (AA/bisAA 30:0.5), TBE, stained with ethidium bromide and quantified using G-box and GeneTools analysis software (Syngene) or PhosphorImager (Typhoon-Trio, GE Healthcare).

For native gel electrophoresis, 120 ng of D20HssCh and D20HcnCh conjugates were loaded on 1% agarose gel (Sigma), TBE, stained with ethidium bromide and visualized using G-box (Syngene).

2.8. Cell culture and transfection

Homo sapiens osteosarcoma 143B cells and primary skin fibroblasts from a patient, bearing mtDNA point mutation in the *ND5* gene (A13514G) at 30% heteroplasmy level [8], were cultivated at 37 °C and 5% CO_2 in MEM (Sigma) containing 1 g/l glucose, supplemented with 10% foetal calf serum (Gibco), 100 U/ml penicillin, 100 μg/ml streptomycin, uridine (50 mg/l) and fungizone (2.5 mg/l) (Gibco). For carrier-free transfection with the lipophilic conjugates labelled with ATTO-565, osteosarcoma 143B cells (2 cm^2) were washed with PBS, Opti-MEM Reduced Serum Medium (Gibco) containing conjugates at 10–100 nM final concentration was added and cell were cultivated 15 h at 37 °C and 5% CO_2, then the medium was changed to MEM. Non-conjugated oligoribonucleotide D20H was used as a control. Transfection procedure did not lead to detectable decrease of viability of the cells. Efficiency of transfection was evaluated by flow cytometry using CyFlow® Space (*Partec*). More than 10,000 cells from each sample were analysed using Flowing Software 2.5.1 (Perttu Terho, Turku Centre for Biotechnology).

2.9. Fluorescent confocal microscopy

For confocal microscopy, osteosarcoma 143B cells cultivated in 2 cm^2 chambers slide (Lab-Tek) were transfected with ATTO-565 or FITC labelled RNA-cholesterol conjugates. At different time periods after transfections, living cells were stained with 100 nM Mito-Tracker Green or Deep Red correspondingly for 30 min at 37 °C, washed and imaged in MEM without red phenol. For chloroquine treatment, transfected cells were cultivated in MEM containing 100 μM chloroquine for 5 h, then the medium was changed to MEM. LSM 780 confocal microscope (Zeiss) was used in conjunction with Zen imaging software and images acquired with a Zeiss 63×/1.40 oil immersion objective. The excitation/emission laser wavelengths were 488 nm (green channel) and 555 nm (red channel). Images were analysed using ImageJ [22] and MosaicSuit plugin [23].

2.10. Heteroplasmy test

Patient fibroblasts bearing mtDNA point mutation in the *ND5* gene (A13514G) at 30% heteroplasmy level were incubated with 70 nM, 150 nM, 1 μM and 2 μM (final concentration) of D20HcnCh conjugate for 15 h, cultivated 2 days in MEM, then a second transfection was performed in the same conditions. Conjugated oligonucleotide HF-KSS: GGTCTTTACAGTGCTTACTTCTCGAGCCCCCTACAGGGCTCCA with antireplicative part corresponding to KSS deletion, which was previously shown to be imported into mitochondria but cannot anneal to mtDNA [4,24] was used as a control. In various post-transfection time periods, cellular DNA was isolated, and heteroplasmy level analysis was performed as described previously [8], using fluorescently labelled primer 5′-FITC-CATACCTCTCACTTCAACCTCC-3′ (Eurogentec). Briefly, the heteroplasmy level was analysed by restriction fragment length polymorphism on a 125-bp PCR fragment encompassing the mutation site, where A13514G mutation creates an HaeIII-specific cleavage site. The HaeIII-digested fragments were separated on a 10% PAGE and quantified using Typhoon-Trio Imager (GE Healthcare). For each cellular DNA sample, PCR amplification has been performed in triplicates, and each PCR reaction has been digested, separated on a 10% PAGE and quantified at least twice.

2.11. Statistical analysis

Results of mitochondrial uptake and heteroplasmy test were statistically processed using the one-way ANOVA, followed by the Duncan's test, values of $p \leq 0.05$ (*), $p \leq 0.001$ (***) were considered to be statistically significant. IBM SPSS software v.22 has been used for analysis. Data are expressed as mean ± S.D. for at least 3 independent experiments.

3. Results

3.1. Lipophilic conjugates of oligoribonucleotides

To establish a carrier-free transfection of human cells with small RNA molecules, we used an anti-replicative RNA (referred to as D20H) targeting a point mutation in ND5 gene, previously demonstrated to be imported into mitochondria and able to decrease the heteroplasmy level in human cybrid cells and patient fibroblasts [8]. This small RNA was conjugated with cholesterol through a biodegradable disulfide bond (D20HssCh, Fig. 1). For this, oligoribonucleotides synthesized according to the phosphoramidite method were 5′-thiol-modified and conjugated with

cholesteryl N-[2-(2-pyridyldisulfonyl)ethyl]carbamate (compound **5**, Fig. 1B). Since the length of the linker between the RNA and lipophilic residue significantly influenced the cellular accumulation of siRNA conjugates [13], we designed a molecule containing 6 carbon atoms, S–S bridge and another two carbon atoms between 5′-nucleotide of RNA and cholesterol residue (Fig. 2A). Purified lipophilic oligoribonucleotide was analysed by ESI-TOF mass spectrometry. The calculated molecular weight was in agreement with the measured value, confirming the structure of the isolated product.

Cleavage of the S–S bond by glutathione (GSH) treatment can be detected by separation of molecules bearing or not a cholesterol residue by denaturating PAGE (Fig. 2B). After 3 h incubation at 37° in buffer containing 5 μM GSH (corresponding to GSH concentration in blood), the S–S bond was not significantly cleaved (Fig. 2B). Upon the increase of GSH concentration up to 5 mM (corresponding to GSH concentration in cytosol of mammalian cells [25]), S–S bond reduction was detected in 50% of molecules, indicating that the conjugate of oligoribonucleotide with cholesterol through a disulfide bond should be rapidly cleaved after delivery into cytoplasm.

Another type of biodegradable linker is a hydrazone bond, which can be cleaved in acidic conditions of certain cellular compartments including endosomes [15]. To obtain an optimal balance between the hydrazone bond lability under acidic conditions and stability under neutral conditions, we used the combination of an aromatic aldehyde with an aliphatic acyl hydrazide [15] (Fig. 1A). We designed a linker containing 2 carbon atoms, hydrazone bridge and another 6 carbon atoms between 5′-nucleotide of RNA and cholesterol residue (Fig. 3A).

For this, hydrazino 6- (cholesteryloxycarbonylamino) hexanoate (compound **3**, Fig. 1A) was synthesized and conjugated to D20H RNA. Lability of the resulted hydrazone bond was tested at various pH conditions, demonstrating that the hydrazone link is stable at pH 6.6 and above, while at pH 6.0 it was completely cleaved in 24 h. At more acidic pH (5.6 and below), cholesterol residue was quickly cut from oligoribonucleotide (50% and 90% of molecules were hydrolysed in 2.5 h at pH 6 and 5.6 respectively) (Fig. 3). Therefore, the conjugate of oligoribonucleotide with cholesterol through a hydrazone bond (referred to as D20HcnCh) should be stable during the cell transfection procedure (pH 7.4), and then would be cleaved inside the endosomes, thus facilitating the release and further mitochondrial import of the RNA moiety.

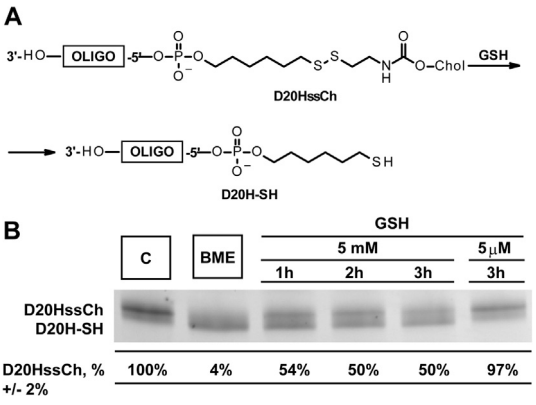

Fig. 2. Cleavage of disulfide bond in D20HssCh conjugate in presence of glutathione (GSH). A, Structure of D20HssCh conjugate and its reduced form D20H-SH. B, Gel electrophoresis analysis of the conjugate treated with GSH as indicated above the panel. Quantification of the portion of D20ssCh (upper band) expressed as mean ± S.D. for 3 independent experiments is shown below the lanes.

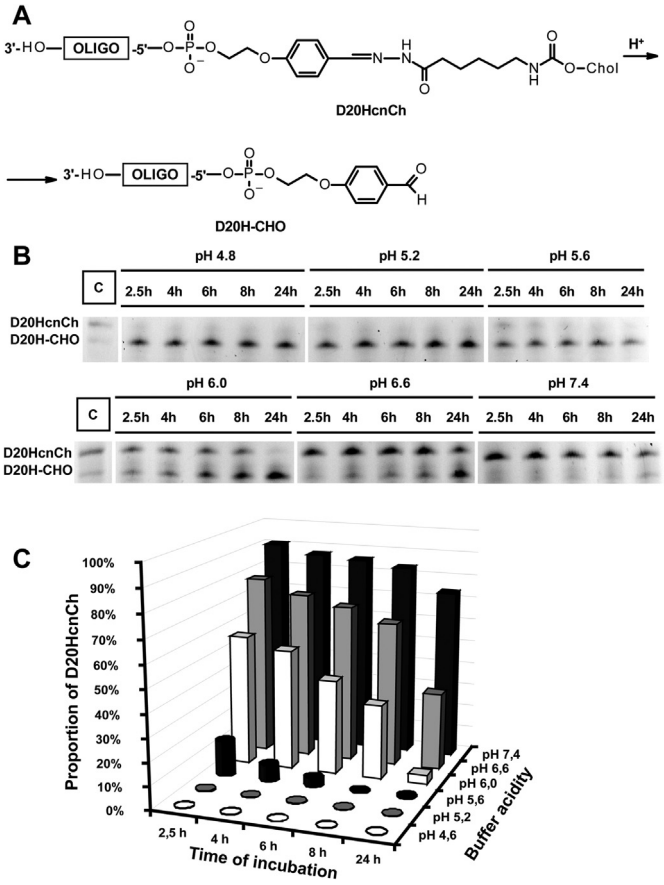

Fig. 3. Hydrazone bond cleavage in D20HcnCh conjugate. A, Structure of D20HcnCh conjugate and its cleaved form D20H-CHO. B, Gel electrophoresis analysis of the hydrolysis products after incubation of the conjugate at various pH during 2.5, 4, 6, 8 and 24 h (as indicated above the panels). Bands corresponding to the full size conjugate (upper band) and the product of its acid hydrolysis (lower band) are indicated at the left. C, Quantification of the full size conjugate (%, axis Y) depending on pH and the time of incubation.

3.2. Cellular uptake of lipophilic conjugates

To detect and quantify the cellular uptake of RNA conjugated with cholesterol, 3′-end of the oligoribonucleotide was labelled with fluorescent compound ATTO-565. Carrier-free transfection of cultured human cells was performed by incubation of osteosarcoma 143B cells with increasing concentrations of RNA conjugated with cholesterol and a non-conjugated oligoribonucleotide D20H used as a control. Efficiency of transfection was measured using cytofluorometry (Fig. 4A,B). The data demonstrate that non-conjugated RNA can not penetrate the cultured human cells. In the same conditions, cellular delivery of RNA conjugated with cholesterol through a disulfide bond (D20HssCh) was detectable but rather inefficient, the fluorescence exceeding the maximum level of cell auto-fluorescence was detected in less than 10% of cells. In contrast to poor uptake obtained for D20HssCh, D20H RNA conjugated through a hydrazone bond (D20HcnCh) was rather efficiently internalized by cells. Percentage of transfected cells reached a plateau of 90 ± 2% after 15 h of incubation with 70 nM D20HcnCh (Fig. 4C).

Fluorescent confocal microscopy images also demonstrated a low internalization of D20HssCh molecules and efficient accumulation of D20HcnCh in the cytoplasm of transfected cells (Fig. 5).

To explain the low level of D20HssCh delivery, we tested the stability of the both conjugates in conditions used for transfection

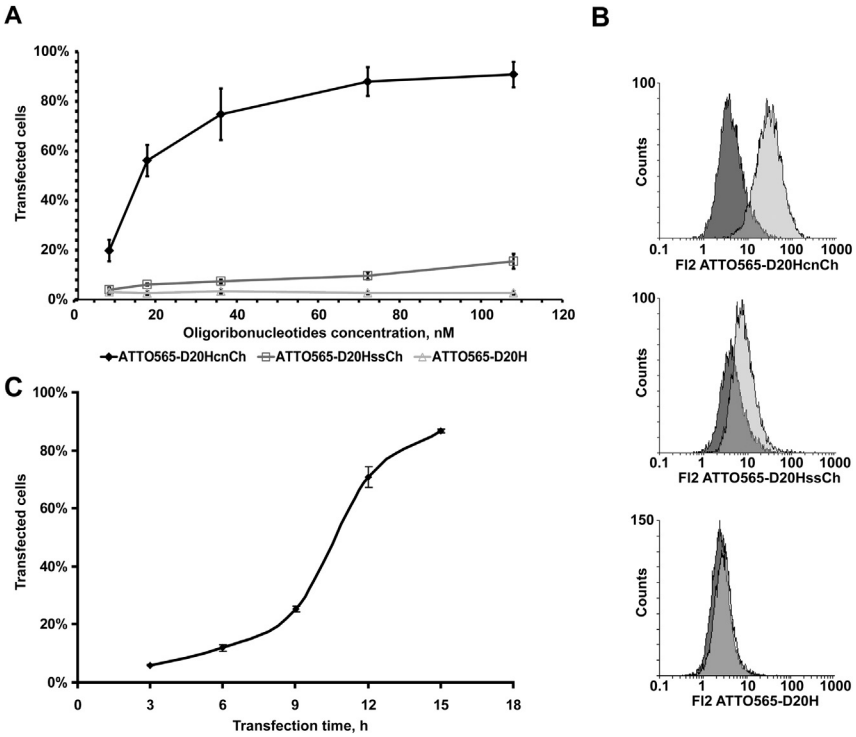

Fig. 4. Cellular uptake of ATTO-labelled lipophilic conjugates estimated by flow cytometry. A, percentage of ATTO-positive 143B cells in the population after 15 h incubation with increased concentrations of conjugates (indicated below). Non-conjugated oligoribonucleotide D20H was used as a control. B, an example of flow cytometry analysis, cells were incubated 15 h with 70 nM ATTO-D20HcnCh (above), ATTO-D20HssCh (middle panel) or ATTO-D20H (lower panel). In dark grey, signal corresponding to auto-fluorescence of non-transfected cells. C, the percentage of ATTO-positive 143B cells in the population after incubation with 70 nM D20HcnCh during various periods of time (indicated below). More than ten thousand events were counted in each sample; mean values from three independent experiments are presented.

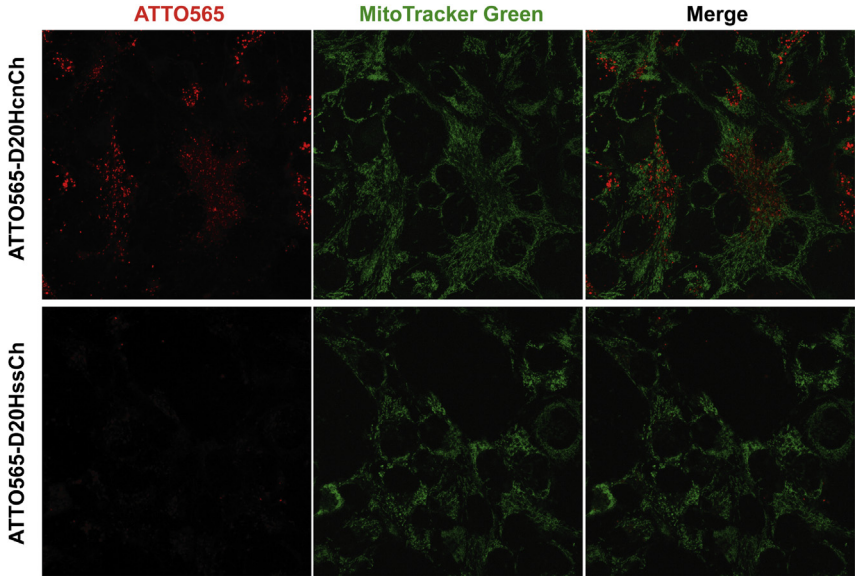

Fig. 5. Cellular uptake of ATTO-labelled lipophilic conjugates analysed by fluorescent confocal microscopy of 143B cells after 15 h incubation with ATTO-D20HcnCh or ATTO-D20HssCh as indicated at the left. Mitochondria were stained with MitoTracker Green (indicated above the panel).

and could not detect any significant degradation (data not shown). Thus, a cause of a low efficacy of transfection with RNA conjugate containing disulfide bond remained unclear. One could hypothesize a self-assembling of this conjugate into micelle-like particles where cholesterol residue and the linker form hydrophobic core shielded by water-soluble RNA [26]. This suggestion has been supported by the comparison of the mobility of both conjugates, D20HssCh and D20HcnCh, in a native agarose gels, demonstrating that an important part of the disulfide-containing conjugate is present in the form a slow-migrating compound. In contrast, for the hydrazone-containing conjugate we detected two bands, corresponding to monomeric and dimeric forms of D20HcnCh, but no aggregation into micelle-like particles was observed (Fig. 6). Thus, the ability of RNA conjugated with cholesterol to form an aggregate clearly

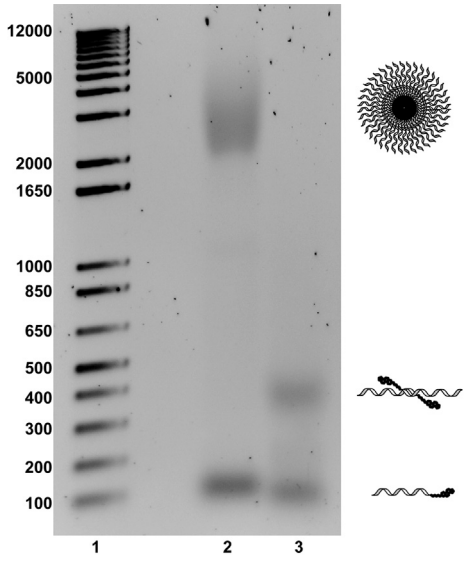

Fig. 6. Aggregation of D20HssCh molecules in native conditions. Agarose gel analysis of the lipophilic conjugates. 1, DNA ladder, size of fragments is indicated at the left; 2, D20HssCh; 3, D20HcnCh. Schematic representation of the monomeric and dimeric RNA conjugates and their aggregation into micelle-like particles is shown at the right.

correlated with the level of its cellular uptake (see also Discussion section).

Further experiments were performed with cells transfected with D20HcnCh conjugate.

3.3. *Mitochondrial targeting and anti-replicative capacity of D20H RNA*

We used optimized conditions for the carrier-free cell transfection with D20HcnCh conjugate (15 h of incubation with 70 nM D20HcnCh) to check if the RNA-component of the internalized conjugate can be targeted to mitochondria. For this, we used confocal laser scanning microscopy of living 143B cells. D20HcnCh was labelled with fluorescein (FITC) at 3′-end, mitochondrial network stained by MitoTracker Deep Red, and co-localization of fluorescent signals had been quantified and statistically analysed (Fig. 7). The data clearly show that the FITC-labelled molecules were partially (13 ± 3% of the cellular pool) addressed to mitochondria 20–45 h post-transfection, then the co-localization level has been significantly decreased, probably indicating on the RNA degradation in the mitochondrial matrix (Fig. 7A, B). Control experiments with FITC only did not demonstrate significant co-localization with mitochondria (1–2%, not shown).

To check the impact of the hydrazone bond cleavage, which was anticipated to occur in acid conditions inside the endosomes, facilitating the release and mitochondrial import of RNA, we treated the transfected cells with chloroquine, an agent that prevents endosomal acidification, commonly used to study the role of endosomal pH in cellular processes [27]. After 5 h of chloroquine treatment, the level of D20H co-localisation with mitochondria was significantly decreased (Fig. 7). This indicates that the increased endosomal pH, preventing the D20HcnCh hydrazone bond cleavage, resulted in the decreased amount of D20H RNA molecules released from the membrane-bound conjugate with cholesterol and therefore accessible for the mitochondrial targeting.

To prove that the released D20H RNA still possessed the anti-replicative activity inside the mitochondria, we performed the carrier-free transfection of patient fibroblasts bearing the pathogenic point mutation in ND5 gene of mtDNA. In various post-transfection time periods, cellular DNA was isolated, and the proportion between normal and mutant mitochondrial genomes (so called heteroplasmy level) was measured by cleavage of the PCR amplicon (Fig. 8). A small but significant decrease of the mutant mtDNA proportion has been detected in the transfected fibroblasts, but not in the control cells cultivated in the same conditions. The same shift of heteroplasmy was obtained in fibroblasts transfected with D20HcnCh conjugate at concentrations 150 nM, 1 μM and 2 μM, indicating that 150 nM concentration of D20HcnCh can be sufficient for the antireplicative effect. Control conjugated oligonucleotide bearing an antireplicative part corresponding to KSS deletion, previously shown to be imported into mitochondria but not capable to anneal to mtDNA [4,24], did not induce a decrease of the heteroplasmy in the transfected fibroblasts (Fig. 8).

These data indicate that the conjugation with cholesterol through hydrazone bond can be useful for a carrier-free delivery of therapeutic anti-replicative RNA into mitochondria of human cells.

4. Discussion

RNA therapeutics is an emerging class of innovative medicine. In recent years, significant progress has been made to overcome some of the obstacles associated with *in vivo* delivery of RNA [28]. Lipid nanoparticles represent one of the most advanced technological platforms [29], together with the rapidly developing approach of molecular conjugates, as triple acetyl-galactosamine conjugates and combination of backbone neutralization with cell-penetrating peptides [30], or lipophilic conjugates [12,31]. A variety of lipophilic moieties can be conjugated to siRNAs to improve the *in vivo* uptake, the best studied one is cholesterol. Mechanistically, cholesterol-modified siRNAs interact with serum lipoprotein particles and the uptake is dependent upon cellular lipoprotein and other *trans*membrane receptors [12]. Recently reported data demonstrate that the adsorption of siRNA lipophilic conjugates on the cell surface and their subsequent transport into the cells could occur via the mechanism of endocytosis. It was suggested that two main factors might determine the efficacy of adsorption of the conjugates on the cell surface: the hydrophobicity of the conjugates and the distance between negatively charged cellular membrane and anionic siRNA [13]. The long aliphatic linker in the conjugate structure provides an optimal distance between the cellular membrane and siRNA moiety, along with an increase of the hydrophobicity of the conjugates. Taking into account these data, we synthesized mitochondrially imported RNAs conjugated to cholesterol through the linker containing 8 aliphatic $-CH_2-$ units.

Another important point is that chemical modifications introduced into RNA molecules should not interfere with their subcellular localization and therapeutic function. In case of siRNA duplexes, a lipophilic residue can be conjugated to the sense strand, which is destroyed upon the cell delivery by RISC complex. Anti-replicative RNAs are expected to be targeted into mitochondrial matrix and to stall the mutant mitochondrial genomes replication [4]. The lipophilic cholesterol residue could impede its mitochondrial import. In fact, human mitochondria possess a system facilitating the transport of cholesterol from the outer mitochondrial membrane to the inner one. This transport is necessary for cholesterol metabolization to pregnenolone, the precursor of all steroid hormones [32]. Translocator protein of the outer mitochondrial membrane TSPO consists of five *trans*membrane helices forming a channel-like structure that may accommodate the import of lipophilic molecules into mitochondria and contains a recognition motif with high affinity to cholesterol [33]. Therefore, the cholesterol residue can be recognized by TSPO and translocated through the outer mitochondrial membrane. In this case, RNA molecule conjugated with cholesterol would be trapped on the

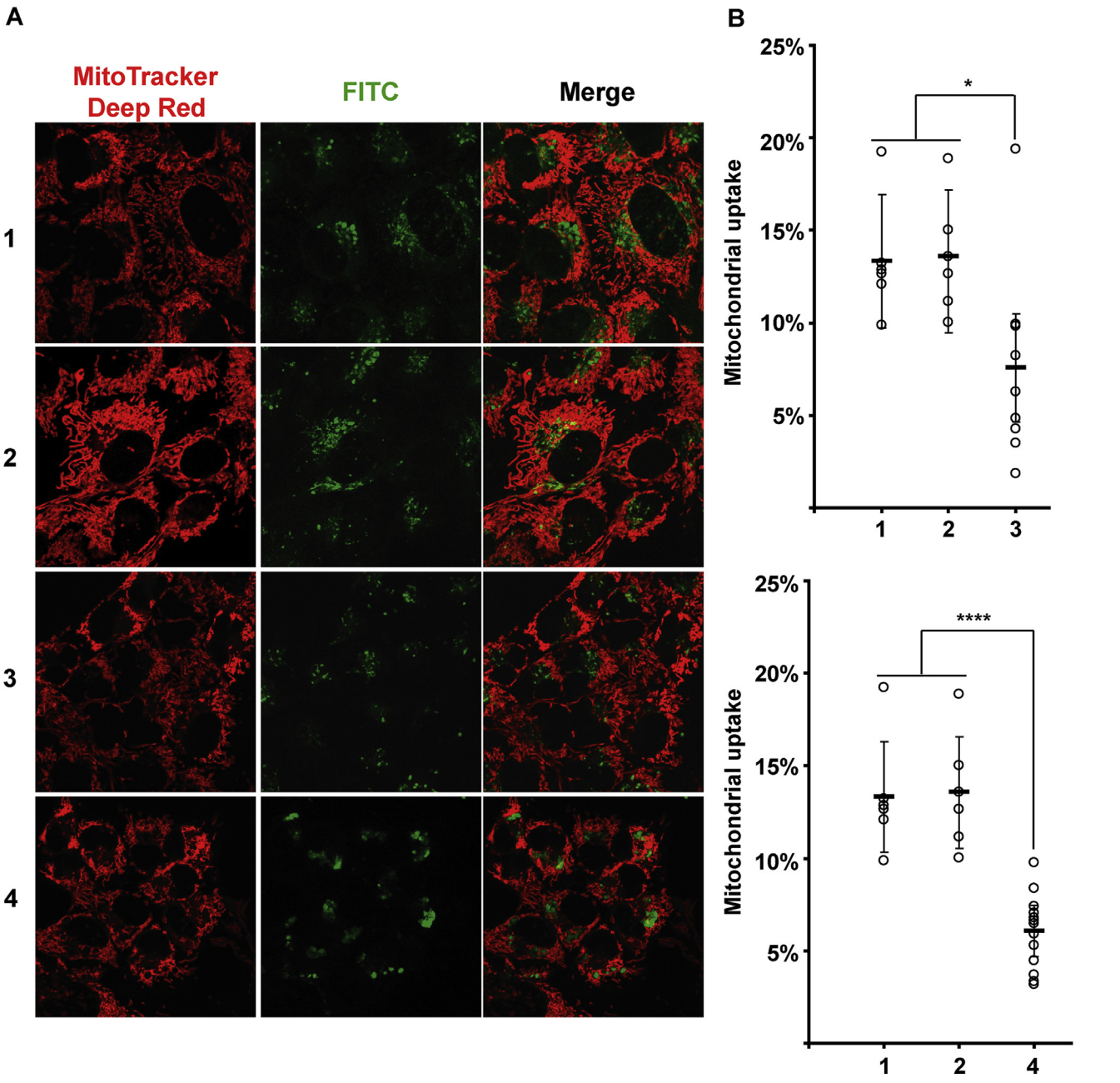

Fig. 7. Mitochondrial targeting of D20H RNA evaluated by fluorescent confocal microscopy. A, confocal microscopy images of 143B cells incubated with FITC-D20HcnCh (green signal), 20 h (**1**), 45 h (**2**) and 70 h (**3**) post-transfection; (**4**), cells were incubated with FITC-D20HcnCh for 15 h, treated with chloroquine for 5 h and analysed 45 h post-transfection. Mitochondrial network was visualized by MitoTracker DeepRed staining. B, quantification of RNA co-localization with mitochondria, estimated as the percentage of green fluorescence signal co-localized with red fluorescence for 6–14 optical sections. The data were statistically processed using the one-way ANOVA, followed by the Duncan's test. Significant differences between cells: *, $p < 0.05$; ****, $p < 0.001$.

outer membrane and, probably, could not be addressed into mitochondrial matrix. To avoid this problem, we introduced a cleavable linker between RNA and cholesterol residue. We expected that the linkers (disulfide or hydrazone bonds) should be stable during cell transfection procedure and cleaved upon internalizing of the conjugate in the cytoplasm [15]. Mammalian cells uptake of extracellular macromolecules proceeds through endocytosis, leading (for the most of endocytosis pathways) to formation of vesicle-like structures that fuse with early endosomes characterised by a reduced pH (6.0–6.6, compared to a physiological pH 7.2–7.4) [34]. The pH drops further during endosomal processing, reaching 5.0 at the late endosomal stage. Therefore, we supposed that the hydrazone bond between RNA and cholesterol moieties would be cleaved inside the endosome, while the disulfide bond should be cleaved after release of the conjugate into the cytoplasm. In both cases, this should permit the mitochondrial targeting of the therapeutic RNA.

Unexpectedly, our data revealed a very low level of cellular uptake for RNA conjugated with cholesterol through a disulfide bond (D20HssCh) compared to RNA conjugated through a hydrazone bond (D20HcnCh). The cause of low efficacy of transfection with RNA conjugate containing disulfide bond remains unclear. It had been demonstrated that siRNAs conjugated through disulfide

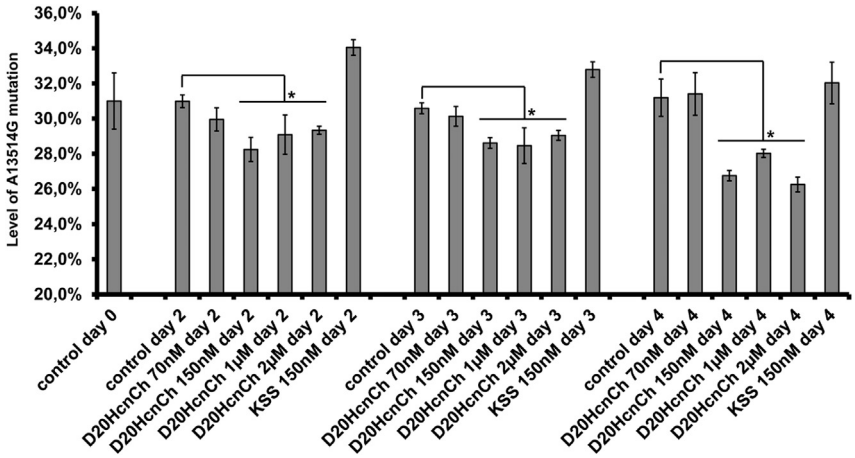

Fig. 8. The effect of D20HcnCh on the heteroplasmy level in transfected patient fibroblasts bearing A13514G mutation in mtDNA. Time dependence of heteroplasmy level after two consecutive transfections with various concentrations of D20HcnCh conjugate (indicated below the graphs) or in the control cells cultivated in the same conditions without transfection. KSS, cells transfected with a control conjugated oligonucleotide which cannot anneal to mtDNA. Data are expressed as mean ± S.D. for 3 independent experiments. Significant differences between control and transfected cells were calculated by one-way ANOVA, followed by Duncan's test (*, $p < 0.05$).

bond were rather efficient in knockdown [35], however, the level of cell transfection had not been estimated. As a possible explanation of a low transfection, we can hypothesize a self-assembling of the disulfide-containing conjugate into micelle-like particles (Fig. 6) where cholesterol residue and the linker form hydrophobic core shielded by water-soluble RNA. Soft micellar nanoparticles assembly from DNA–cholesterol conjugates have been recently described [36]. Cholesterol residues shielded inside the particles could not bind the cell surface receptors and, therefore, penetrate the cells.

In case of the hydrazone containing conjugate, the ratio between hydrophobic and hydrophilic parts of the molecule should be more significant than in case of disulfide linker. This would prevent the self-assembling of conjugates into micelle-like particles [26], thus increasing the amount of molecules available for the cell delivery. Therefore, the hydrazone containing conjugate D20HcnCh demonstrated an efficient carrier-free cellular uptake. The level of its consequent co-localisation with mitochondria was estimated as 13 ± 3% of the D20H cellular pool (Fig. 7). We suppose that this value is limited by the endosomal escape of the D20H RNA after the hydrazone bond cleavage in acidic conditions. However, the treatment of transfected cell with chloroquine, one of the endosomal escape agents, which was supposed to facilitate the disruption of the endosomal membrane due to proton sponge mechanism [37], in fact decreased the mitochondrial targeting of D20H RNA (Fig. 7). These data indicate that the conjugated molecules D20HcnCh were anchored in the endosomal membranes by the cholesterol residue. Since the endosomal pH has been increased by the chloroquine treatment, the hydrazone bond between the cholesterol and RNA components was not cleaved, and RNA could not be released into cytoplasm even after the disruption of endosomes.

Noteworthy, the moderate mitochondrial import of D20H RNA still allowed detection of its anti-replicative activity. Even the small decrease of heteroplasmy level (Fig. 8) can be important to obtain a curative effect of mitochondrial dysfunctions in human cells, since only high levels of mutations in human mtDNA become pathogenic [6], while a small reduction of the mutant DNA load can provide significant clinical improvement [38].

The present study was done on cultivated primary fibroblasts from patients affected by mitochondrial dysfunction and represents a proof of concept that the biodegradable cholesterol–RNA conjugates can be used for reducing a level of mtDNA pathological mutation. The next step towards the therapy would be to use more developed models. Concerning *ex vivo* therapies, our system could be applied to treatment of specific tissue of affected patient which can be cultivated and treated following by re-injection, for instance, marrow tissue in the case of Pearson marrow-pancreas syndrome, associated with deletions in mtDNA [39]. Another model would be the *trans*mitochondrial lines of mice embryonic stem cells carrying heteroplasmic mtDNA mutations in genes coding for respiratory subunits or tRNA [40,41]. These ES cells, able to differentiate into neurons or myoblasts, provide therefore a model to study the cellular pathophysiology and the effect of the therapeutic RNA delivery on defined tissue types. Our system could be also applied to test the possibility of induced heteroplasmy change in embryos bearing mutations in mtDNA. Recently an alternative approach of mtDNA cleavage by mitoTALENs has been successfully applied to mice embryos [42]. Our system could be also tested for the possibility to induce a heteroplasmy change in embryos bearing pathogenic mutations in mtDNA, which would be helpful for the preimplantation genetic diagnosis and possible therapy [43].

Only few murine models carrying mitochondrial DNA mutations have been described to date, due to difficulties in producing transgenic mice carrying pathogenic mtDNA mutations [44]. Heteroplasmic mutations described in transgenic mice include lifelong expanding deletion in mtDNA ("mito-mice", [45]) or a point mutation in the $tRNA^{Lys}$ gene mimicking the MERRF syndrome-associated mutation [41]. If even it has not be possible to completely recapitulate, in these murine lines, the human symptoms associated with mtDNA defects, the model could be used for the validation of the antireplicative strategy. To improve the *in vivo* delivery of cholesterol–RNA conjugates, we are planning to design and synthesize conjugated molecules containing various nucleotide and inter-nucleotide modifications which can improve the stability of anti-replicative RNA moieties and promote their tissue distribution and cellular uptake.

5. Conclusion

We have developed an approach of carrier-free targeting of the mitochondrially importable RNA into living human cells. RNA conjugated with cholesterol through a hydrazone bond represents a new type of conjugates containing pH-triggered link. Anti-replicative RNA conjugated to cholesterol through a hydrazone

bond was efficiently internalized by cells, partially co-localized with mitochondrial network and induced a decrease in the proportion of mitochondrial genomes bearing a pathogenic point mutation. We believe that the present study represents a further step towards the development of RNA therapeutics against incurable mitochondrial diseases.

Acknowledgements

The authors are grateful to Dr. Agnès Rötig (*Hôpital Necker-Enfants Malades, Paris)* for providing the patient fibroblasts, to Jérôme Mutterer (*IBMP, Strasbourg*) for helpful assistance in confocal microscopy, to Philippe Wolf (*IBMC, Strasbourg*) for ESI-TOF-MS analysis, to Anne-Marie Heckel for excellent technical assistance and to Dr. Anna Smirnova and Dr. Alexandre Smirnov for helpful discussions.

This work has been published under the framework of the LABEX ANR-11-LABX-0057_MITOCROSS and is supported by the state managed by the French National Research Agency as part of the Investment for the Future program. The work was also supported by CNRS (Centre National de Recherche Scientifique); University of Strasbourg, the LIA (International Associated Laboratory) ARN-mitocure and by the grant number 14-14-00697 of the Russian Research Foundation (RSCF). ID was supported by ARCUS-SUPRACHEM and MitoCross PhD fellowships.

References

[1] J.C. Burnett, J.J. Rossi, RNA-based therapeutics: current progress and future prospects, Chem. Biol. 19 (2012) 60–71.
[2] G. Tavernier, O. Andries, J. Demeester, N.N. Sanders, S.C. De Smedt, J. Rejman, mRNA as gene therapeutic: how to control protein expression, J. Control Release 150 (2011) 238–247.
[3] O. Kolesnikova, et al., Selection of RNA aptamers imported into yeast and human mitochondria, RNA 16 (2010) 926–941.
[4] C. Comte, et al., Mitochondrial targeting of recombinant RNAs modulates the level of a heteroplasmic mutation in human mitochondrial DNA associated with Kearns Sayre Syndrome, Nucleic Acids Res. 41 (2013) 418–433.
[5] E. Ruiz-Pesini, et al., An enhanced MITOMAP with a global mtDNA mutational phylogeny, Nucleic Acids Res. 35 (2007) D823–D828.
[6] D.C. Wallace, Mitochondrial DNA mutations in disease and aging, Environ. Mol. Mutagen. 51 (2010) 440–450.
[7] R.W. Taylor, D.M. Turnbull, Mitochondrial DNA mutations in human disease, Nat. Rev. Genet. 6 (2005) 389–402.
[8] Y. Tonin, et al., Modeling of antigenomic therapy of mitochondrial diseases by mitochondrially addressed RNA targeting a pathogenic point mutation in mitochondrial DNA, J. Biol. Chem. 289 (2014) 13323–13334.
[9] J. Zhou, K.T. Shum, J.C. Burnett, J.J. Rossi, Nanoparticle-based delivery of RNAi therapeutics: progress and challenges, Pharm. – Basel Switz. 6 (2013) 85–107.
[10] H. Lv, S. Zhang, B. Wang, S. Cui, J. Yan, Toxicity of cationic lipids and cationic polymers in gene delivery, J. Control Release 114 (2006) 100–109.
[11] J. Winkler, Oligonucleotide conjugates for therapeutic applications, Ther. Deliv. 4 (2013) 791–809.
[12] C. Wolfrum, et al., Mechanisms and optimization of in vivo delivery of lipophilic siRNAs, Nat. Biotechnol. 25 (2007) 1149–1157.
[13] N.S. Petrova, et al., Carrier-free cellular uptake and the gene-silencing activity of the lipophilic siRNAs is strongly affected by the length of the linker between siRNA and lipophilic group, Nucleic Acids Res. 40 (2012) 2330–2344.
[14] R.L. Letsinger, G.R. Zhang, D.K. Sun, T. Ikeuchi, P.S. Sarin, Cholesteryl-conjugated oligonucleotides: synthesis, properties, and activity as inhibitors of replication of human immunodeficiency virus in cell culture, Proc. Natl. Acad. Sci. U. S. A. 86 (1989) 6553–6556.
[15] K.R. West, S. Otto, Reversible covalent chemistry in drug delivery, Curr. Drug Discov. Technol. 2 (2005) 123–160.
[16] C. Yamada, A. Khvorova, R. Kaiser, E. Anderson, D. Leake. Duplex oligonucleotide complexes and methods for gene silencing by RNA interference. Google Patents, (2013).
[17] M. Tognolini, et al., Structure-activity relationships and mechanism of action of Eph-ephrin antagonists: interaction of cholanic acid with the EphA2 receptor, ChemMedChem 7 (2012) 1071–1083.
[18] G.T. Zugates, D.G. Anderson, S.R. Little, I.E. Lawhorn, R. Langer, Synthesis of poly(beta-amino ester)s with thiol-reactive side chains for DNA delivery, J. Am. Chem. Soc. 128 (2006) 12726–12734.
[19] M. Sugahara, M. Uragami, X. Yan, S.L. Regen, The structural role of cholesterol in biological membranes, J. Am. Chem. Soc. 123 (2001) 7939–7940.
[20] L. Bellon, Oligoribonucleotides with 2′-O-(tert-butyldimethylsilyl) groups, Curr. Protoc. Nucleic Acid Chem. (2001). Chapter 3: Unit 3 6.
[21] I. Dovydenko, et al., Mitochondrial targeting of recombinant RNA, Methods Mol. Biol. 1265 (2015) 209–225.
[22] C.A. Schneider, W.S. Rasband, K.W. Eliceiri, NIH Image to ImageJ: 25 years of image analysis, Nat. Methods 9 (2012) 671–675.
[23] A. Rizk, et al., Segmentation and quantification of subcellular structures in fluorescence microscopy images using Squassh, Nat. Protoc. 9 (2014) 586–596.
[24] A. Gowher, A. Smirnov, I. Tarassov, N. Entelis, Induced tRNA import into human mitochondria: implication of a host aminoacyl-tRNA-synthetase, PLoS One 8 (2013) e66228.
[25] C. Hwang, A.J. Sinskey, H.F. Lodish, Oxidized redox state of glutathione in the endoplasmic reticulum, Science 257 (1992) 1496–1502.
[26] D.A. Balazs, W. Godbey, Liposomes for use in gene delivery, J. Drug Deliv. 2011 (2011) 326497.
[27] M. Rutz, et al., Toll-like receptor 9 binds single-stranded CpG-DNA in a sequence- and pH-dependent manner, Eur. J. Immunol. 34 (2004) 2541–2550.
[28] A.R. de Fougerolles, Delivery vehicles for small interfering RNA in vivo, Hum. Gene Ther. 19 (2008) 125–132.
[29] M.J. Hope, Enhancing siRNA delivery by employing lipid nanoparticles, Ther. Deliv. 5 (2014) 663–673.
[30] B.R. Meade, et al., Efficient delivery of RNAi prodrugs containing reversible charge-neutralizing phosphotriester backbone modifications, Nat. Biotechnol. 32 (2014) 1256–1261.
[31] M. Raouane, D. Desmaele, G. Urbinati, L. Massaad-Massade, P. Couvreur, Lipid conjugated oligonucleotides: a useful strategy for delivery, Bioconjug. Chem. 23 (2012) 1091–1104.
[32] W.L. Miller, H.S. Bose, Early steps in steroidogenesis: intracellular cholesterol trafficking, J. Lipid Res. 52 (2011) 2111–2135.
[33] L. Jaremko, M. Jaremko, K. Giller, S. Becker, M. Zweckstetter, Structure of the mitochondrial translocator protein in complex with a diagnostic ligand, Science 343 (2014) 1363–1366.
[34] W. De Haes, G. Van Mol, C. Merlin, S.C. De Smedt, G. Vanham, J. Rejman, Internalization of mRNA lipoplexes by dendritic cells, Mol. Pharm. 9 (2012) 2942–2949.
[35] Q. Chen, et al., Lipophilic siRNAs mediate efficient gene silencing in oligodendrocytes with direct CNS delivery, J. Control Release 144 (2010) 227–232.
[36] J.P. Magnusson, F. Fernandez-Trillo, G. Sicilia, S.G. Spain, C. Alexander, Programmed assembly of polymer-DNA conjugate nanoparticles with optical readout and sequence-specific activation of biorecognition, Nanoscale 6 (2014) 2368–2374.
[37] A.K. Varkouhi, M. Scholte, G. Storm, H.J. Haisma, Endosomal escape pathways for delivery of biologicals, J. Control Release 151 (2011) 220–228.
[38] M. Picard, et al., Progressive increase in mtDNA 3243A>G heteroplasmy causes abrupt transcriptional reprogramming, Proc. Natl. Acad. Sci. U. S. A. 111 (2014) E4033–E4042.
[39] E.M. Manea, et al., Pearson syndrome in the neonatal period: two case reports and review of the literature, J. Pediatr. Hematol. Oncol. 31 (2009) 947–951.
[40] D.M. Kirby, et al., Transmitochondrial embryonic stem cells containing pathogenic mtDNA mutations are compromised in neuronal differentiation, Cell Prolif. 42 (2009) 413–424.
[41] A. Shimizu, et al., Mouse somatic mutation orthologous to MELAS A3302G mutation in the mitochondrial tRNA gene confers respiration defects, Biochem. Biophys. Res. Commun. (2015 Sep 14), http://dx.doi.org/10.1016/j.bbrc.2015.09.072 pii: S0006-291X(15)30589-1. (Epub ahead of print).
[42] P. Reddy, et al., Selective elimination of mitochondrial mutations in the germline by genome editing, Cell 161 (2015) 459–469.
[43] S. Monnot, et al., Segregation of mtDNA throughout human embryofetal development: m.3243A>G as a model system, Hum. Mutat. 32 (2011) 116–125.
[44] W. Fan, et al., A mouse model of mitochondrial disease reveals germline selection against severe mtDNA mutations, Science 319 (2008) 958–962.
[45] K. Nakada, J. Hayashi, Transmitochondrial mice as models for mitochondrial DNA-based diseases, Exp. Anim. 60 (2011) 421–431.